catalysts

MDPI

Article

Water Splitting on Multifaceted $SrTiO_3$ Nanocrystals: Computational Study

Maksim Sokolov [1,*], Yuri A. Mastrikov [1,*], Guntars Zvejnieks [1], Dmitry Bocharov [1] and Eugene A. Kotomin [1] and Veera Krasnenko [2]

[1] Institute of Solid State Physics, University of Latvia, Kengaraga 8, LV1063 Riga, Latvia; guntars.zvejnieks@cfi.lu.lv (G.Z.); Dmitrijs.Bocarovs@cfi.lu.lv (D.B.); jevgenijs.kotomins@cfi.lu.lv (E.A.K.)
[2] Institute of Physics, University of Tartu, W.Ostwaldi 1, 50411 Tartu, Estonia; veera.krasnenko@ut.ee
* maksims.sokolovs@cfi.lu.lv (M.S.); yuri.mastrikov@cfi.lu.lv (Y.A.M.)

Abstract: Recent experimental findings suggest that strontium titanate $SrTiO_3$ (STO) photocatalytic activity for water splitting could be improved by creating multifaceted nanoparticles. To understand the underlying mechanisms and energetics, the model for faceted nanoparticles was created. The multifaceted nanoparticles' surface is considered by us as a combination of flat and "stepped" facets. Ab initio calculations of the adsorption of water and oxygen evolution reaction (OER) intermediates were performed. Our findings suggest that the "slope" part of the step showed a natural similarity to the flat surface, whereas the "ridge" part exhibited significantly different adsorption configurations. On the "slope" region, both molecular and dissociative adsorption modes were possible, whereas on the "ridge", only dissociative adsorption was observed. Water adsorption energies on the "ridge" (−1.50 eV) were significantly higher than on the "slope" (−0.76 eV molecular; −0.83 eV dissociative) or flat surface (−0.79 eV molecular; −1.09 eV dissociative).

Keywords: STO; OER; DFT; stepped surface; water splitting

Citation: Sokolov, M.; Mastrikov, Y.A.; Zvejnieks, G.; Bocharov, D.; Kotomin, E.A.; Krasnenko, K. Water Splitting on Multifaceted $SrTiO_3$ Nanocrystals: A Computational Study. *Catalysts* **2021**, *11*, 1326. https://doi.org/10.3390/catal11111326

Academic Editors: Zhenghua Tang, Marc Cretin and Sophie Tingry

Received: 12 October 2021
Accepted: 30 October 2021
Published: 31 October 2021

1. Introduction

Strontium titanate $SrTiO_3$ (STO) is a well-known material for water splitting [1–12]. The process of water adsorption and dissociation was studied in detail [13–15]. The effects of doping are investigated in [16]. Recent developments in nanocrystal synthesis offered materials with enhanced charge separation achieved by heterojunction [17,18], mesocrystallinity [19], or the exposed anisotropic facets [20,21]. Nanoparticles synthesized by Takata et al. [20] were made from STO doped by aluminium and photodeposited cocatalysts Rh/Cr_2O_3 and CoOOH, and demonstrated a quantum efficiency of up to 96% in the range of 350 to 360 nm. Synthesized six and eighteen-facet STO nanocrystals, as described in [21], demonstrated high catalytic activity in water splitting. When doped by Pt and Co_3O_4 on particular facets, these nanoparticles exhibited even higher performance. Such an improvement is attributed to the unique properties of anisotropic facets of the particles.

One of the key properties of a high-performance water splitting material is a low charge recombination rate. Adsorption of water and oxygen evolution reaction (OER) intermediates on stepped surfaces is expected to be qualitatively different than that on flat surfaces. Featuring surfaces of different orientations, the 18-facet nanoparticle provides a natural platform for efficient charge separation. The six-facet nanoparticle is essentially a cube with the {0 0 1} faces. Its edges, however, can be considered as a different reaction area from the {0 0 1} flat parts. Currently, to the best of our knowledge, the structure of the surface of these nanoparticles is described only at the nanoscale. To reveal the properties of different reaction areas of multi-faceted nanoparticles, an atomistic model has to be designed and tested.

In 18-facet STO nanoparticle, the {0 0 1} facets are combined with the facets parallel to the {1 1 0} crystallographic plane. Although for the real material, the surfaces {0 0 1}

and $\{1\,0\,0\}$ are not equivalent [22], for the present study, the distortion of the perovskite structure is irrelevant and the orientation of the surfaces are given relative to the cubic phase. As it was shown in [23], the ideal polar $\{1\,1\,0\}$ surface is unstable. Its stabilization can be achieved by forming steps of the more stable $\{0\,0\,1\}$ orientation [24].

In the present study, we propose an atomistic model of the $\{0\,0\,1\}$ stepped surface, which is relevant to both six as well as eighteen-facet STO nanoparticles. On this surface, we simulate OER, as suggested by Nørskov [25]. The four-step reaction includes adsorption of H_2O, HO^*, O^*, and HOO^* species. The results will be used to perform thermodynamic simulations of the OER to obtain over-potential η^{OER} values.

An extensive investigation of OER on the flat STO surface was performed by Cui et al. [14]. For the flat $\{0\,0\,1\}$, the STO surface of the over-potential value of 0.66 V was obtained.

2. Methods and Computational Details

We performed density functional theory (DFT) calculations using the Vienna Ab initio Simulation Package (VASP) [26–29]. Computational details are listed in Table 1. Relaxed rhombohedral $SrTiO_3$ phase ($R\bar{3}c$) with the optimized lattice constant a_0 of 3.92 Å was used. We compared flat surface and stepped surface, as shown in Figures 1 and 2, respectively. Adsorbate was placed on both terminations of the slab to neutralize the electric dipole moment.

Adsorption energy $E_{\mathrm{ads},\,x}$ for the configuration x was calculated by Equation (1), where E_x is the total energy of the configuration with the adsorbate, E_{surf} is the total energy of the corresponding surface without the adsorbate, E_{H_2O} is the total energy of water, E_{H_2} is the total energy of molecular hydrogen, and coefficients c_1 and c_2 are determined so that the total number of particles on the left hand side of the equation is zero. Factor $\frac{1}{2}$ is a result of the adsorbate being placed on both terminations of the slab. Lower adsorption energy corresponds to the stronger binding.

All figures were created in the VESTA visualization system [30].

$$E_{\mathrm{ads},\,x} = \frac{1}{2}(E_x - (E_{\mathrm{surf}} + c_1 E_{H_2O} + c_2 E_{H_2})) \quad (1)$$

Table 1. Computational details.

Software	VASP 6 [27–29]
Exchange-correlation functional	GGA-PBE [31]
Pseudopotentials	Ultra Soft [32,33] potentials using the Projector Augmented Wave (PAW) method [34,35]
Smearing	Gaussian smearing
Ti-valence configuration	$3p^6 3d^2 4s^2$, valence 10, energy cutoff 222 eV, generated 07.09.2000
Sr-valence configuration	$4s^2 4p^6 5s^2$, valence 10, energy cutoff 229 eV, generated 07.09.2000
O-valence configuration	$2s^2 2p^4$, valence 6, energy cutoff 400 eV, generated 08.04.2002
H-valence configuration	$1s^1$, valence 1, energy cutoff 250 eV, generated 15.06.2001
Spin polarization	Non-spin polarized calculation
Plane wave basis set cut-off	520 eV
Flat surface geometry (Figure 1)	$2a_0 \times 4a_0$ surface cell, seven layers-thick, 20 Å vacuum gap, 144 atoms
Stepped surface geometry (Figure 2)	$2(2a_0 \times 2a_0)$, $2\sqrt{2}a_0$ thickness, 10 Å vacuum gap, 104 atoms
Flat surface k-point mesh	$4 \times 2 \times 2$ Monkhorst-Pack [36]
Stepped surface k-point mesh	$4 \times 4 \times 2$ Monkhorst-Pack [36]

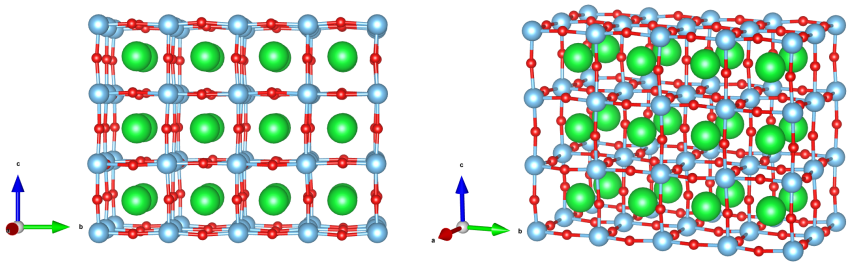

(**a**) (**b**)

Figure 1. Flat surface cell. (**a**) Front view. (**b**) Isometric view.

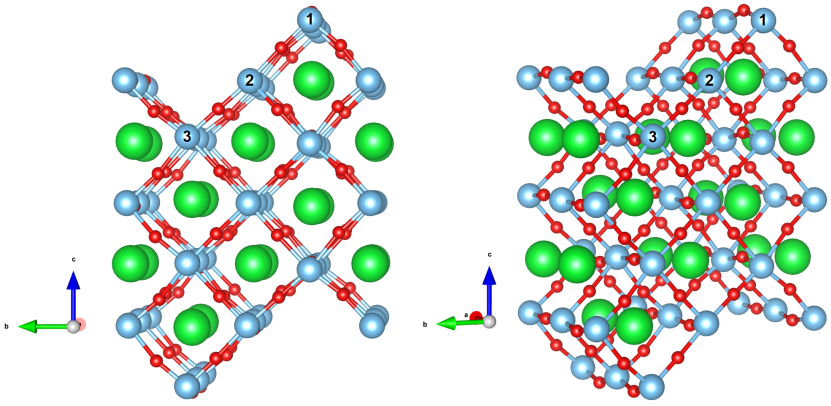

(**a**) (**b**)

Figure 2. Stepped surface cell. The one-ridge adsorption area; two-slope adsorption area; and three-gully adsorption area. (**a**) Front view. (**b**) Isometric view.

3. Results and Discussion

3.1. Water Adsorption

It is important to understand how water adsorption on stepped surfaces distinguishes from that on flat surfaces. On flat surfaces, the most preferable water adsorption site is atop titanium. The stepped model of faceted surfaces features three regions: the ridge, slope, and gully, marked on Figure 2.

On flat surfaces, two adsorption modes are possible: molecular (Figure 3a; $E_{ads} = -0.79$ eV) and dissociative (Figure 3b; $E_{ads} = -1.09$ eV), with dissociative being more energetically favorable, which is in agreement with Reference [13]. In [13], it was demonstrated that there is no significant transition barrier (0.09 eV) between the two adsorption modes. On the stepped surface, the situation is more complex and each adsorption region should be discussed separately.

On the *Slope* region, there are several possible adsorption configurations. The most energetically favorable one is dissociative adsorption along Slope (Figure 4d; $E_{ads} = -0.83$ eV), followed closely by molecular adsorption (Figure 4b,c with E_{ads} of -0.76 eV and -0.71 eV, respectively). Molecular adsorption energy on the slope was loosely dependent on the orientation of water molecules. Dissociation towards the gully or ridge was less favorable (Figure 4e,f with E_{ads} of -0.62 eV and -0.41 eV, respectively). Although, similarly to flat surfaces, one of the possible dissociative configurations on the slope was more favorable than molecular ones, the difference between energies was not as large, thus it cannot be unequivocally concluded, wherein the adsorption mode dominates.

On the *Ridge* region, only one configuration was observed: water dissociation accompanied by spontaneous oxygen vacancy formation (Figure 4a). It also had the lowest adsorption energy (strongest adsorption) of −1.50 eV among all the tested configurations. The investigation of the question regarding whether the ridge breaks down irreversibly or whether the vacancy is healed during subsequent water adsorption is out of scope of this paper.

On the *Gully* region, only one dissociative configuration was found, but only hydrogen was adsorbed, while oxygen was on the slope. Moreover, this configuration had a relatively weak binding (Figure 4g, $E_{ads} = -0.49$ eV), hence we did not investigate it further.

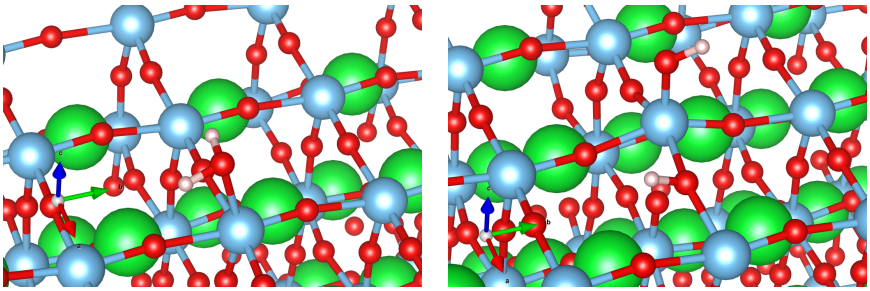

(**a**) (**b**)

Figure 3. Water adsorption configuration on the stepped surface. (**a**) Molecular adsorption on the flat surface: $E_{ads} = -0.79$ eV. (**b**) Dissociative adsorption on the flat surface: $E_{ads} = -1.09$ eV.

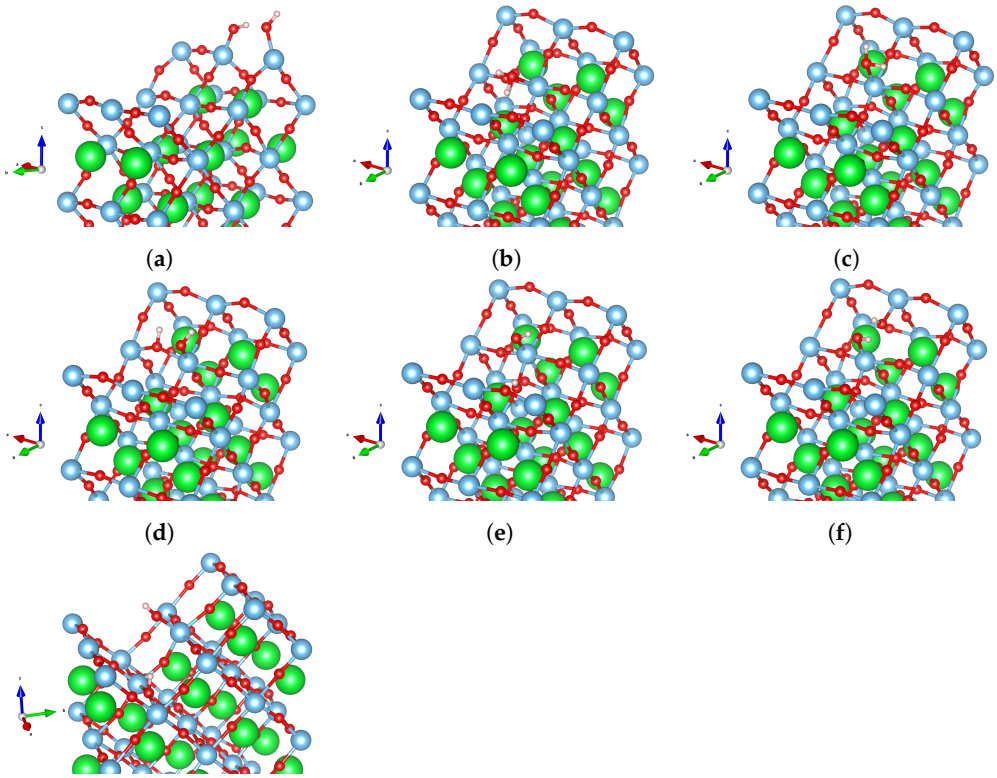

(**a**) (**b**) (**c**)

(**d**) (**e**) (**f**)

(**g**)

Figure 4. Water adsorption configurations on the stepped surface. (**a**) Adsorption on the ridge region. $E_{ads} = -1.50$ eV. (**b**) Molecular adsorption on the slope region with water oriented towards the gully. $E_{ads} = -0.76$ eV. (**c**) Molecular adsorption on the slope region with water oriented towards the ridge. $E_{ads} = -0.71$ eV. (**d**) Dissociative adsorption on the slope region with hydrogen migrated along the slope. $E_{ads} = -0.83$ eV. (**e**) Dissociative adsorption on the slope region with hydrogen migrated towards the gully. $E_{ads} = -0.62$ eV. (**f**) Dissociative adsorption on the slope region with hydrogen migrated towards the ridge. $E_{ads} = -0.41$ eV. (**g**) Dissociative adsorption on the gully region. $E_{ads} = -0.49$ eV.

3.2. Oxygen Evolution Reaction (OER) Intermediates

To perform thermodynamic simulations to estimate STO photo-catalytic activity, it is necessary to compute adsorption energies for oxygen evolution reaction (OER) intermediates: HO^*, O^*, and HOO^*, where the star * denotes the active adsorption site. All energies are compiled in Table 2.

Results for the flat surface are shown in Figure 5. HO^* had only one possible configuration, as shown in Figure 5a. There were two possible configurations for O^*: where oxygen from the adsorbate bonded to surface oxygen, denoted as $O^*_{(O_{surf})}$ (Figure 5b), and where oxygen was atop titanium, denoted as O^* (Figure 5c). The $O^*_{(O_{surf})}$ adsorption energy was much lower (2.87 eV versus 3.52 eV), thus it was more energetically favorable. The HOO^* adsorbate also had two configurations: one where hydrogen bonded to surface oxygen (Figure 5d), denoted as $H_{(O_{surf})}OO^*$, and the other where hydrogen bonded to the adsorbate's oxygen (Figure 5e), denoted as HOO^*. In [14], only the second configuration was mentioned, although its adsorption energy was significantly higher than that of the $H_{(O_{surf})}OO^*$ configuration: 4.24 eV versus 3.64 eV.

The adsorption of intermediates on the slope (Figure 6) was similar to that of the flat surface: only one HO^* configuration (Figure 6a), $O^*_{(O_{surf})}$ (Figure 6b), and O^* (Figure 6c), and two HOO^* configurations, namely $H_{(O_{surf})}OO^*$ (Figure 6d) and HOO^* (Figure 6e) were observed. $O^*_{(O_{surf})}$ was more energetically favorable than O^* (2.93 eV versus 4.11 eV) and $H_{(O_{surf})}OO^*$ was more favorable than HOO^* (3.48 eV versus 4.52 eV), analogous to the flat surface. HO^* on the slope had higher adsorption energy than HO^* on the flat surface (1.35 eV versus 0.77 eV).

Results for the intermediates on the ridge region are shown in Figure 7. For each intermediate, only one adsorption configuration was observed. HO^* (Figure 7a) and HOO^* (Figure 7c), similarly to the water adsorption, were accompanied by spontaneous oxygen vacancy formation, while O^* bonded between surface oxygen and titanium (Figure 7b).

Table 2. Adsorption energies of oxygen evolution reaction (OER) intermediates on different types of surfaces.

Surface Type	HO^*, eV	O^*, eV	HOO^*, eV
Flat surface	0.77 (Figure 5a)	2.87 (Figure 5b)/3.52 (Figure 5c)	3.64 (Figure 5d)/4.24 (Figure 5e)
Slope	1.35 (Figure 6a)	2.93 (Figure 6b)/4.11 (Figure 6c)	3.48 (Figure 6d)/4.52 (Figure 6e)
Ridge	1.24 (Figure 7a)	2.40 (Figure 7b)	3.13 (Figure 7c)

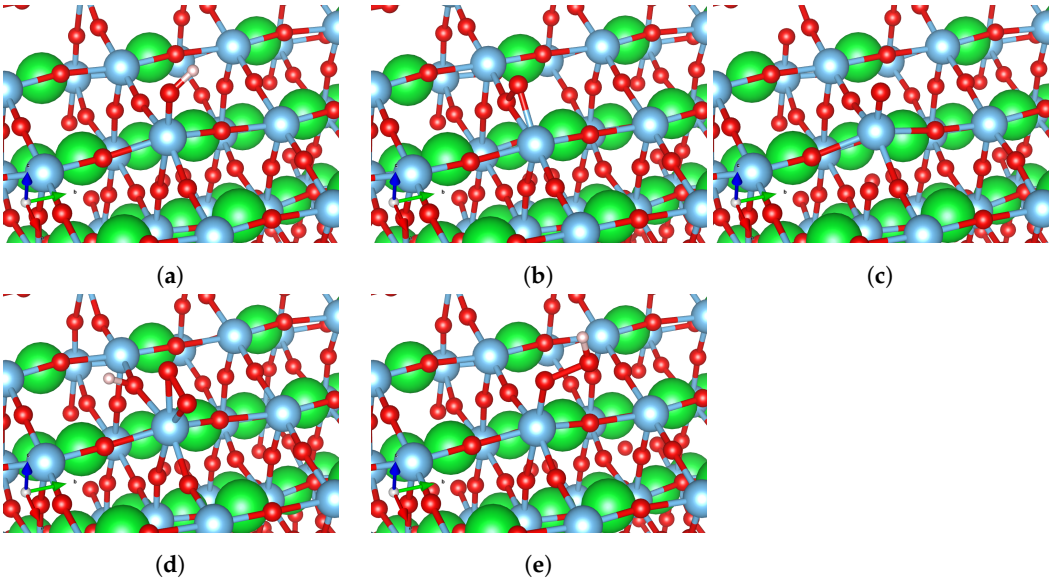

Figure 5. OER intermediates on the flat surface. (**a**) HO^* adsorbate on the flat surface: $E_{ads} = 0.77$ eV. (**b**) $O^*_{(O_{surf})}$ adsorbate on the flat surface: $E_{ads} = 2.87$ eV. (**c**) O^* adsorbate on the flat surface: $E_{ads} = 3.52$ eV. (**d**) $H_{(O_{surf})}OO^*$ adsorbate on the flat surface: $E_{ads} = 3.64$ eV. (**e**) HOO^* adsorbate on the flat surface, standard configuration:
$E_{ads} = 4.24$ eV.

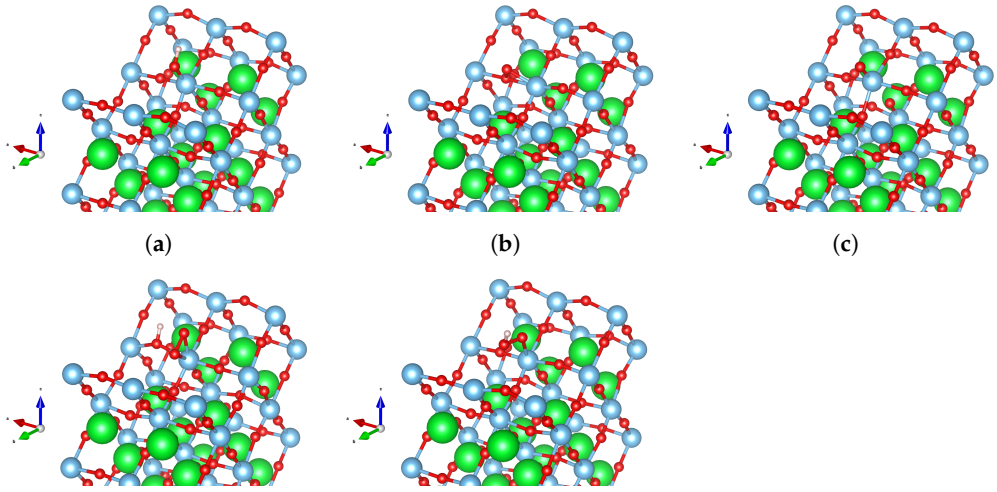

Figure 6. OER intermediates on the slope of the stepped surface. (**a**) HO^* adsorbate on the slope region: $E_{ads} = 1.35$ eV. (**b**) $O^*_{(O_{surf})}$ adsorbate on the slope region: $E_{ads} = 2.93$ eV. (**c**) O^* adsorbate on the slope region: $E_{ads} = 4.11$ eV. (**d**) $H_{(O_{surf})}OO^*$ adsorbate on the slope region: $E_{ads} = 3.48$ eV. (**e**) HOO^* adsorbate on the slope region: $E_{ads} = 4.52$ eV.

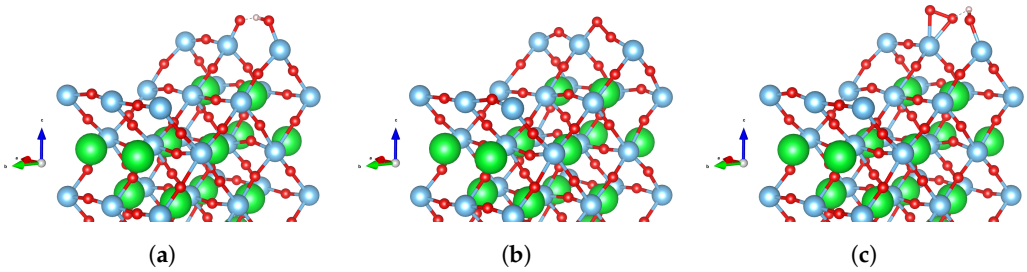

Figure 7. OER intermediates on the ridge of the stepped surface. (**a**) HO^* adsorbate on the ridge region: $E_{ads} = 1.24$ eV. (**b**) O^* adsorbate on the ridge region: $E_{ads} = 2.40$ eV. (**c**) HOO^* adsorbate on the ridge region: $E_{ads} = 3.13$ eV.

4. Conclusions

We have performed a detailed investigation of water adsorption and oxygen evolution reaction (OER) intermediate adsorption on strontium titanate $SrTiO_3$ flat and stepped surfaces. In contrast to the flat surface, the stepped surface, a significant part of which comprises the ridge region, demonstrated high adsorption energies as well as pronounced structural transformations caused by the adsorbate. Our findings suggest that:

- The ridge region permits dissociative water adsorption only, accompanied by spontaneous formation of oxygen vacancy;
- Results for the flat surface are in agreement with other computational studies [13];
- On the slope region, both molecular and dissociative adsorption modes are possible;
- Adsorption of both water and its intermediates on the slope region is similar to that on flat surfaces;
- Except for atomic hydrogen, no adsorption was observed on the gully region; and
- There are different adsorption configurations of OER intermediates possible on flat surfaces and slope regions.

Author Contributions: Conceptualization, Y.A.M. and E.A.K.; data curation, M.S. and V.K.; formal analysis, M.S.; funding acquisition, D.B. and E.A.K.; investigation, M.S., Y.A.M., G.Z. and V.K.; methodology, Y.A.M., D.B. and E.A.K.; project administration, D.B. and E.A.K.; resources, Y.A.M. and E.A.K.; software, M.S.; supervision, Y.A.M., D.B. and E.A.K.; validation, M.S., Y.A.M., G.Z. and V.K.; visualization, M.S.; writing—original draft, M.S.; writing—review and editing, Y.A.M., D.B. and E.A.K. All authors have read and agreed to the published version of the manuscript.

Funding: The financial support of M-ERA.NET2 Sun2Chem project is greatly acknowledged by E.K. Authors thank Marjeta Maček Kržmanc and Chi-Sheng Wu, for the fruitful discussions. The financial support of FLAG-ERA JTC project To2Dox is acknowledged by Y.A.M. This paper is based upon the work from COST Action 18234, supported by COST (European Cooperation in Science and Technology). The support is greatly acknowledged by Y.A.M. and V.K. The grant No. 1.1.1.2/VIAA/1/16/147 (1.1.1.2/16/I/001) under the activity of Post-doctoral research aid is greatly acknowledged by M.S. and D.B.

Acknowledgments: The Institute of Solid State Physics, University of Latvia (Latvia) as the Centre of Excellence has received funding from the European Union's Horizon 2020 Frame-work Programme H2020-WIDESPREAD-01-2016-2017-Teaming Phase2 under grant agreement No. 739508, project CAMART^2. The computer resources were provided by the Stuttgart Supercomputing Center (project DEFTD 12939) and Latvian Super Cluster (LASC).

Conflicts of Interest: The authors declare no conflict of interest.

References

1. Kato, H.; Kudo, A. Visible-Light-Response and Photocatalytic Activities of TiO_2 and $SrTiO_3$ Photocatalysts Codoped with Antimony and Chromium. *J. Phys. Chem. B* **2002**, *106*, 5029–5034. [CrossRef]
2. Miyauchi, M.; Nakajima, A.; Watanabe, T.; Hashimoto, K. Photocatalysis and Photoinduced Hydrophilicity of Various Metal Oxide Thin Films. *Chem. Mater.* **2002**, *14*, 2812–2816. [CrossRef]
3. Konta, R.; Ishii, T.; Kato, H.; Kudo, A. Photocatalytic Activities of Noble Metal Ion Doped $SrTiO_3$ under Visible Light Irradiation. *J. Phys. Chem. B* **2004**, *108*, 8992–8995. [CrossRef]
4. Yu, S.C.; Huang, C.W.; Liao, C.H.; Wu, J.C.; Chang, S.T.; Chen, K.H. A novel membrane reactor for separating hydrogen and oxygen in photocatalytic water splitting. *J. Membr. Sci.* **2011**, *382*, 291–299. [CrossRef]
5. Kato, H.; Kobayashi, M.; Hara, M.; Kakihana, M. Fabrication of $SrTiO_3$ exposing characteristic facets using molten salt flux and improvement of photocatalytic activity for water splitting. *Catal. Sci. Technol.* **2013**, *3*, 1733. [CrossRef]
6. Wang, B.; Shen, S.; Guo, L. $SrTiO_3$ single crystals enclosed with high-indexed 023 facets and 001 facets for photocatalytic hydrogen and oxygen evolution. *Appl. Catal. B Environ.* **2015**, *166–167*, 320–326. [CrossRef]
7. Ham, Y.; Hisatomi, T.; Goto, Y.; Moriya, Y.; Sakata, Y.; Yamakata, A.; Kubota, J.; Domen, K. Flux-mediated doping of $SrTiO_3$ photocatalysts for efficient overall water splitting. *J. Mater. Chem. A* **2016**, *4*, 3027–3033. [CrossRef]
8. Foo, G.S.; Hood, Z.D.; Wu, Z. Shape Effect Undermined by Surface Reconstruction: Ethanol Dehydrogenation over Shape-Controlled $SrTiO_3$ Nanocrystals. *ACS Catal.* **2018**, *8*, 555–565. [CrossRef]
9. Li, D.; Yu, J.C.C.; Nguyen, V.H.; Wu, J.C.; Wang, X. A dual-function photocatalytic system for simultaneous separating hydrogen from water splitting and photocatalytic degradation of phenol in a twin-reactor. *Appl. Catal. B Environ.* **2018**, *239*, 268–279. [CrossRef]
10. Kampouri, S.; Stylianou, K.C. Dual-Functional Photocatalysis for Simultaneous Hydrogen Production and Oxidation of Organic Substances. *ACS Catal.* **2019**, *9*, 4247–4270. [CrossRef]
11. Kanazawa, T.; Nozawa, S.; Lu, D.; Maeda, K. Structure and Photocatalytic Activity of PdCrOx Cocatalyst on $SrTiO_3$ for Overall Water Splitting. *Catalysts* **2019**, *9*, 59. [CrossRef]
12. Saleem, Z.; Pervaiz, E.; Yousaf, M.U.; Niazi, M.B.K. Two-dimensional materials and composites as potential water splitting photocatalysts: A review. *Catalysts* **2020**, *10*, 464. [CrossRef]
13. Guhl, H.; Miller, W.; Reuter, K. Water adsorption and dissociation on $SrTiO_3$ (001) revisited: A density functional theory study. *Phys. Rev. B Condens. Matter Mater. Phys.* **2010**, *81*, 155455. [CrossRef]
14. Cui, M.; Liu, T.; Li, Q.; Yang, J.; Jia, Y. Oxygen Evolution Reaction (OER) on Clean and Oxygen Deficient Low-Index $SrTiO_3$ Surfaces: A Theoretical Systematic Study. *ACS Sustain. Chem. Eng.* **2019**, *7*, 15346–15353. [CrossRef]
15. Holmström, E.; Spijker, P.; Foster, A.S. The interface of $SrTiO_3$ and H_2O from density functional theory molecular dynamics. *Proc. R. Soc. A Math. Phys. Eng. Sci.* **2016**, *472*. [CrossRef]
16. Chen, H.C.; Huang, C.W.; Wu, J.C.S.; Lin, S.T. Theoretical Investigation of the Metal-Doped $SrTiO_3$ Photocatalysts for Water Splitting. *J. Phys. Chem. C* **2012**, *116*, 7897–7903. [CrossRef]
17. Afroz, K.; Moniruddin, M.; Bakranov, N.; Kudaibergenov, S.; Nuraje, N. A heterojunction strategy to improve the visible light sensitive water splitting performance of photocatalytic materials. *J. Mater. Chem. A* **2018**, *6*, 21696–21718. [CrossRef]
18. Maček Kržmanc, M.; Daneu, N.; Čontala, A.; Santra, S.; Kamal, K.M.; Likozar, B.; Spreitzer, M. $SrTiO_3/Bi_4Ti_3O_{12}$Nanohetero structural Platelets Synthesized by Topotactic Epitaxy as Effective Noble-Metal-Free Photocatalysts for pH-Neutral Hydrogen Evolution. *ACS Appl. Mater. Interfaces* **2021**, *13*, 370–381. [CrossRef] [PubMed]
19. Li, X.; Yu, J.; Jaroniec, M. Hierarchical photocatalysts. *Chem. Soc. Rev.* **2016**, *45*, 2603–2636. [CrossRef]
20. Takata, T.; Jiang, J.; Sakata, Y.; Nakabayashi, M.; Shibata, N.; Nandal, V.; Seki, K.; Hisatomi, T.; Domen, K. Photocatalytic water splitting with a quantum efficiency of almost unity. *Nature* **2020**, *581*, 411–414. [CrossRef]

21. Mu, L.; Zhao, Y.; Li, A.; Wang, S.; Wang, Z.; Yang, J.; Wang, Y.; Liu, T.; Chen, R.; Zhu, J.; et al. Enhancing charge separation on high symmetry $SrTiO_3$ exposed with anisotropic facets for photocatalytic water splitting. *Energy Environ. Sci.* **2016**, *9*, 2463–2469. [CrossRef]
22. Tomio, T.; Miki, H.; Tabata, H.; Kawai, T.; Kawai, S. Control of electrical conductivity in laser deposited $SrTiO_3$ thin films with Nb doping. *J. Appl. Phys.* **1994**, *76*, 5886–5890. [CrossRef]
23. Noguera, C. Polar oxide surfaces. *J. Phys. Condens. Matter* **2000**, *12*, R367–R410. [CrossRef]
24. Bachelet, R.; Valle, F.; Infante, I.C.; Sánchez, F.; Fontcuberta, J. Step formation, faceting, and bunching in atomically flat $SrTiO_3$ (110) surfaces. *Appl. Phys. Lett.* **2007**, *91*, 251904. [CrossRef]
25. Man, I.C.; Su, H.Y.; Calle-Vallejo, F.; Hansen, H.A.; Martínez, J.I.; Inoglu, N.G.; Kitchin, J.; Jaramillo, T.F.; Nørskov, J.K.; Rossmeisl, J. Universality in Oxygen Evolution Electrocatalysis on Oxide Surfaces. *ChemCatChem* **2011**, *3*, 1159–1165. [CrossRef]
26. Kresse, G.; Hafner, J. Ab initio molecular dynamics for liquid metals. *Phys. Rev. B* **1993**, *47*, 558–561. [CrossRef]
27. Kresse, G.; Hafner, J. Ab initio molecular-dynamics simulation of the liquid-metal–amorphous-semiconductor transition in germanium. *Phys. Rev. B* **1994**, *49*, 14251–14269. [CrossRef] [PubMed]
28. Kresse, G.; Furthmüller, J. Efficiency of ab-initio total energy calculations for metals and semiconductors using a plane-wave basis set. *Comput. Mater. Sci.* **1996**, *6*, 15–50. [CrossRef]
29. Kresse, G.; Furthmüller, J. Efficient iterative schemes for ab initio total-energy calculations using a plane-wave basis set. *Phys. Rev. B* **1996**, *54*, 11169–11186. [CrossRef]
30. Momma, K.; Izumi, F. VESTA 3 for three-dimensional visualization of crystal, volumetric and morphology data. *J. Appl. Crystallogr.* **2011**, *44*, 1272–1276. [CrossRef]
31. Perdew, J.P.; Burke, K.; Ernzerhof, M. Generalized Gradient Approximation Made Simple. *Phys. Rev. Lett.* **1996**, *77*, 3865–3868. [CrossRef] [PubMed]
32. Vanderbilt, D. Soft self-consistent pseudopotentials in a generalized eigenvalue formalism. *Phys. Rev. B* **1990**, *41*, 7892–7895. [CrossRef]
33. Kresse, G.; Hafner, J. Norm-conserving and ultrasoft pseudopotentials for first-row and transition elements. *J. Phys. Condens. Matter* **1994**, *6*, 8245–8257. [CrossRef]
34. Blöchl, P.E. Projector augmented-wave method. *Phys. Rev. B* **1994**, *50*, 17953–17979. [CrossRef]
35. Kresse, G.; Joubert, D. From ultrasoft pseudopotentials to the projector augmented-wave method. *Phys. Rev. B* **1999**, *59*, 1758–1775. [CrossRef]
36. Monkhorst, H.J.; Pack, J.D. Special points for Brillouin-zone integrations. *Phys. Rev. B* **1976**, *13*, 5188–5192. [CrossRef]